IRAQI JOURNAL OF MATERIALS
Volume (4) Issue (2) April-June 2025, pp. 89-94

Characteristics of Palladium-Decorated Porous Silicon Structures Fabricated by Electrostatic Injection Technique

Yang Hu Liang, Zhang Boo Wei, Ming Liao Dong

College of Applied Sciences, National Taiwan University of Science and Technology, Taipei City 106335, TAIWAN (R.O.C.)

Abstract
In this work, porous silicon layer formed by Photoelectrochemical etching on the surface of p-type silicon substrate was decorated with palladium nanoparticles applied over the porous layer by the electrostatic injection technique. The structural and surface morphological characteristics of the decorated structure were reasonably modified when compared to those of the as-prepared porous structure. The porosity, porous layer thickness and pore diameter were found reasonably depending on the current density passing through the circuit used for the Photoelectrochemical etching process. However, both the porosity and porous layer thickness showed saturation limit at high current densities, while the pore diameter was found to increase continuously with increasing current density.

Keywords: Porous silicon, Etching technique, Palladium dopants; Nanoparticles
Received: 11 January 2025; **Revised:** 02 March 2025; **Accepted:** 17 March 2025; **Published:** 1 April 2025

1. Introduction

Photodetectors fabricated from porous silicon structures have gained significant attention due to their unique optical and electrical properties [1]. Porous silicon, with its high surface area, tunable porosity, and adjustable bandgap, enables enhanced light absorption and efficient photodetection across various wavelengths. These structures are particularly advantageous for miniaturized, cost-effective optoelectronic devices. Their integration into photodetectors enhances sensitivity and response time, making them ideal for applications like optical sensing, environmental monitoring, medical diagnostics, and telecommunications [2-4]. Moreover, their compatibility with silicon-based technologies simplifies integration into existing systems, paving the way for innovative, high-performance devices in fields demanding precise and efficient light detection capabilities [5,6].

Palladium is a silvery-white, ductile, and malleable metal belonging to the platinum group of elements. It has a high melting point of 1554°C and excellent corrosion resistance, making it stable in various environments [7]. Palladium exhibits remarkable catalytic properties, particularly in facilitating hydrogenation and oxidation reactions. It readily absorbs hydrogen, forming palladium hydride, a unique property used in hydrogen storage and sensing applications [8]. Chemically, palladium is relatively inert but can form compounds with halogens, sulfur, and carbon [9]. Its electrical conductivity and ability to form alloys make it invaluable in electronics, jewelry, and catalytic converters for reducing harmful emissions in automobiles [10].

Palladium nanoparticles exhibit unique properties such as high surface area, excellent catalytic activity, and remarkable chemical stability, making them highly valuable in various applications [11-13]. They are widely used in catalysis for hydrogenation, oxidation, and carbon-carbon coupling reactions, as well as in sensors, fuel cells, and biomedical fields. Their small size and quantum effects enhance their performance in energy conversion and storage [14,15]. Common preparation methods include chemical reduction, where palladium salts are reduced to nanoparticles using reducing agents, and physical methods like laser ablation and thermal decomposition. Other techniques, such as green synthesis using plant extracts, emphasize eco-friendly nanoparticle production [16-18].

The electrostatic injection technique is a versatile method for embedding nanoparticles into porous structures with high precision and uniform distribution [19-21]. This technique utilizes electrostatic forces to drive charged nanoparticles into the pores of a substrate [22,23]. A nanoparticle suspension is typically exposed to an electric field, which directs the charged particles toward the porous material, ensuring efficient penetration and adhesion within the structure. This method offers advantages such as

© All Rights Reserved

controlled loading, minimal agglomeration, and enhanced nanoparticle integration [24,25]. It is widely used in applications like catalysis, drug delivery, and sensor fabrication, where the uniform embedding of nanoparticles significantly improves performance and functionality [26-28].

2. Experimental Work

The chemical reduction method is the most common and widely used technique for synthesizing palladium nanoparticles. This method involves reducing palladium salts (e.g., palladium chloride or palladium acetate) in the presence of reducing agents such as sodium borohydride, ascorbic acid, or hydrazine. In this process, stabilizing agents (e.g., polyvinylpyrrolidone, citrate, or surfactants) are often used to prevent nanoparticle agglomeration. The reaction is typically conducted in an aqueous or organic solvent under controlled temperature and pH conditions. This method is favored for its simplicity, scalability, and ability to produce uniformly sized nanoparticles with high purity and controlled shapes. Figure (1) shows schematically the experimental stages of preparation of porous silicon layer on the p-type silicon substrates, the electrostatic injection of palladium nanoparticles on the prepared porous silicon layer, and finally the architecture of the fabricated PANI-coated Pd-decorated porous silicon structure.

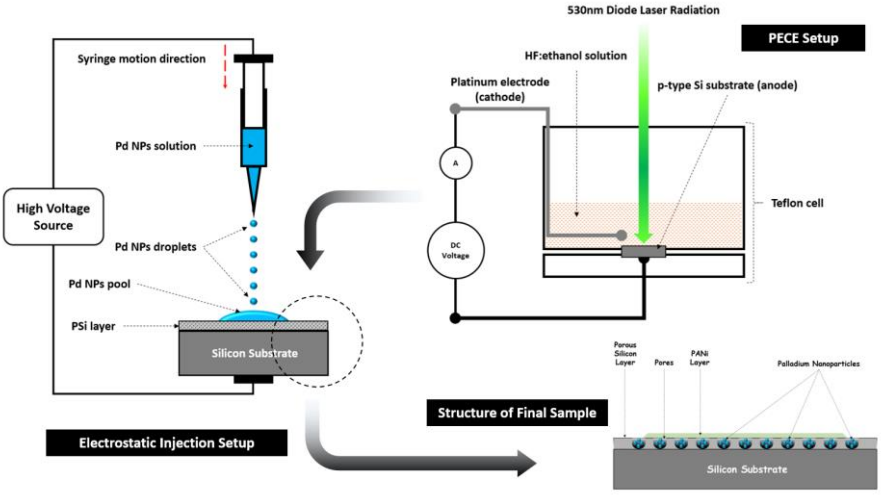

Fig. (1) Schematic diagram of the experimental setup stages used in this work to prepare PANI-coated Pd-decorated porous silicon structure formed on p-type Si substrate

To prepare palladium nanoparticles using the chemical reduction method, the following experimental procedure is typically employed. Palladium precursor (e.g., palladium chloride, $PdCl_2$), reducing agent (e.g., sodium borohydride, ascorbic acid, or hydrazine), stabilizing agent (e.g., polyvinylpyrrolidone (PVP) or citrate), and a solvent (usually water or ethanol) were used. A 10^3 M concentration of the palladium salt is dissolved in the chosen solvent to form the precursor solution. The solution is stirred to ensure complete dissolution. A stabilizing agent is added to the precursor solution to prevent the aggregation of nanoparticles and maintain stability during synthesis. The reducing agent is prepared separately and added dropwise to the precursor solution under constant stirring. The reduction reaction converts Pd^{2+} ions into palladium atoms, which nucleate and grow into nanoparticles. The reaction is typically carried out at room temperature or slightly elevated temperatures, depending on the reducing agent used. The pH of the solution may be adjusted to optimize the reaction. The progress of nanoparticle formation can be monitored using techniques like UV-visible spectroscopy, where the characteristic surface plasmon resonance (SPR) peak indicates the presence of palladium nanoparticles. The nanoparticles are separated by centrifugation, washed with solvents (e.g., ethanol or water) to remove unreacted precursors and byproducts, and then dried under vacuum or at room temperature. This method is simple, cost-effective, and produces nanoparticles with controlled sizes and shapes suitable for various applications, such as catalysis and sensing.

The preparation of a porous silicon (PS) layer on a silicon substrate using the photo-electro-chemical etching (PECE) method involves the following. A p-type silicon with a specific orientation ⟨100⟩ was used. The etching solution contains hydrofluoric acid (HF) mixed with ethanol or deionized water in a specific ratio (3:1). Light source is a 530nm laser diode with 1mW power used for illumination during

© All Rights Reserved

etching to generate electron-hole pairs in the semiconductor. The electrochemical setup includes a Teflon or glass cell, a platinum counter electrode, and a silicon wafer as the working electrode. A dc power supply was sued to control the applied voltage or current. A constant voltage or current is applied using a power supply, initiating the etching process. So, the photogenerated holes migrate to the silicon-electrolyte interface, enabling the selective dissolution of silicon in the presence of HF.

The silicon wafer was cleaned to remove organic and inorganic contaminants. Common cleaning steps include washing with acetone, ethanol, and deionized water, and then dipping in a dilute HF solution to remove the native oxide layer. The silicon wafer was mounted in the cell with its polished side exposed to the etching solution. A seal (O-ring) was used to ensure that only the desired area is exposed to the electrolyte. The wafer acts as the anode, and a platinum wire or mesh serves as the cathode. Ethanol helps improve wettability and ensures uniform etching by reducing bubble formation.

The etched wafer was thoroughly rinsed with ethanol and deionized water to remove residual HF and other byproducts. The wafer was dried using nitrogen gas or air-drying. This method allows precise control over the pore size, depth, and porosity, making it suitable for applications in sensors, optoelectronics, and biomedical devices. The resulting PS layer was characterized for its morphology, thickness, and porosity using techniques such as x-ray diffraction (XRD) and field-emission scanning electron microscopy (FE-SEM). A polyaniline (PANI) layer was applied over the Pd-decorated PSi layer to enhance its stability and protect it from environmental factors like humidity, oxidation, and contamination. The PANI layer acts as a protective coating, preserving the catalytic properties of palladium while preventing degradation and improving the longevity of the device.

3. Results and Discussion

Figure (2) shows the XRD patterns of the porous silicon layer before and after the decoration with palladium nanoparticles. The characteristic peak of porous silicon located at 33.5° corresponding to the (100) crystal plane, according to the JCPDS card no. 96-101-1061, was the only peak seen in the XRD pattern of the porous silicon layer, which highlights the advantage of the photoelectrochemical etching process used in this work to prepare highly pure porous structure with no traces for the crystalline silicon or other materials. After decoration with Pd nanoparticles, the peak of porous silicon (PSi) is apparently seen in the XRD pattern in addition to the appearance of two peaks located at 40.48° and 67.85° corresponding to the crystal planes of (111) and (220), respectively, of the face-centered cubic (f.c.c.) structure of palladium nanoparticles according to the JCPDS card no. 05-0681 [29,30].

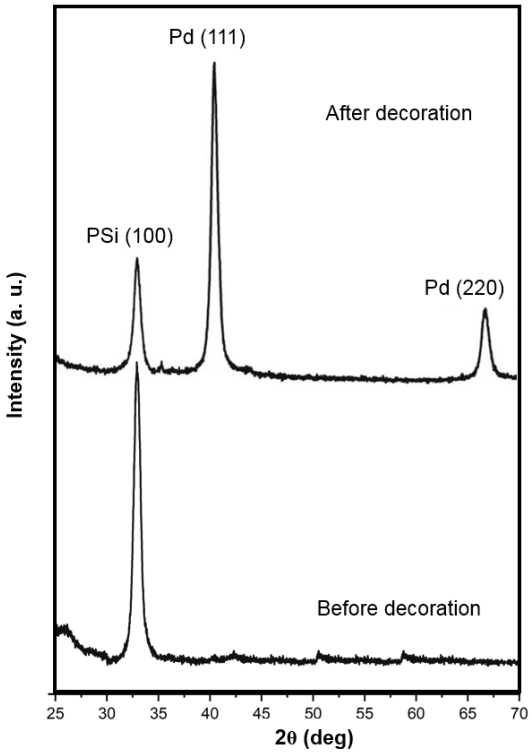

Fig. (2) XRD patterns of the porous silicon structure before and after decoration with Pd nanoparticles

© All Rights Reserved

Figure (3) shows the FE-SEM images of the porous silicon layer before and after the decoration with palladium nanoparticles. The porous structure formed on the silicon substrate is apparently seen in Fig. (3a) with different 3D geometries of the pores. However, individual pores can be reasonably recognized. In Fig. (3b), the distribution of Pd nanoparticles is apparent too as the nanoparticles penetrate inside the pores while other nanoparticles cover the surface of the porous layer and cumulate on the area between the pores. In both cases, the Pd nanoparticles can modify the characteristics of the porous silicon layer due to two synergetic effects. In the first effect, the nanoparticles embedded inside the pores contribute to increase the electrical conductivity of the porous silicon layer by forming inter-band states with the energy gap of the porous silicon [31]. In the second effect, the nanoparticles covering the surface outside the pores form a Schottky-like structure that contribute to the optoelectronic performance of the whole fabricated structure [32].

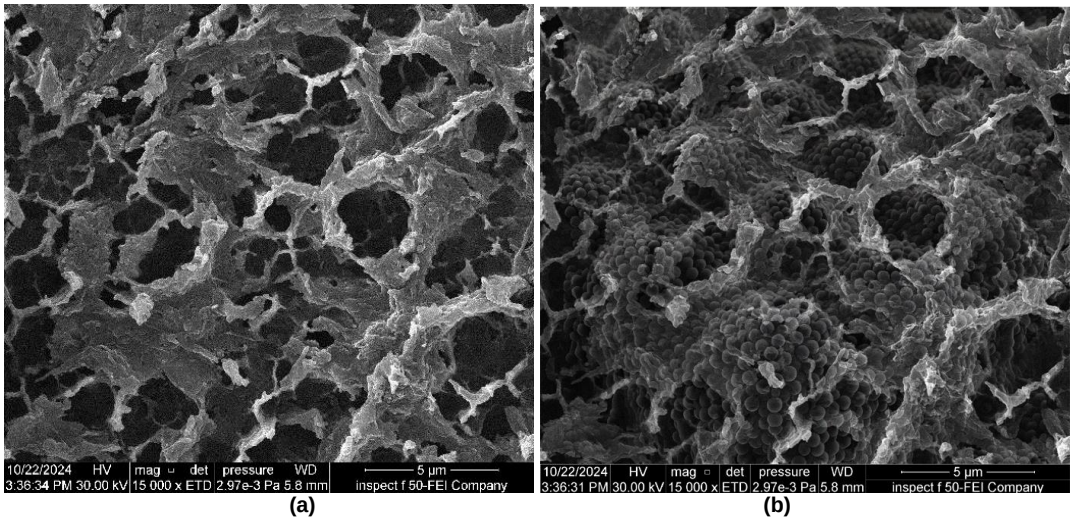

(a) **(b)**

Fig. (3) FE-SEM images of (a) porous silicon layer, and (b) Pd-decorated porous silicon structure

The structural features of bare PSi layers such as the pore shape, their dimensions and wall sizes between neighboring pores depend intensively the applied current density. The surface morphological of PSi was investigated by the field-emission scanning electron microscopy (FE-SEM). The initial PSi layer appears as a pore-like cylindrical with a random distribution of pores. The increase in pore size has also led to an overlapping of the pores which disfigured their shapes. The accumulation of electron-hole pairs within the porous layer may be responsible for the pore diameters [33]. By increasing the etching current density, the pore diameters increased. It ranged between 0.4 and 3.4 µm as the current density was ranging from 10 to 40 mA/cm^2 with 30% distribution of 1.64 µm. The porosity (P%) of the porous silicon layer after etching was calculated gravimetrically using the following equation:

$$P(\%) = \frac{m_1 - m_2}{m_1 - m_3} \quad (1)$$

where m_1 is the weight of silicon substrate before etching, m_2 is the weight after etching, and m_3 is the weight after removing the porous silicon layer by treatment the sample with 5 M NaOH for 5 min

The thickness (d) of porous silicon layer can be determined by the following equation:

$$d = \frac{m_1 - m_3}{A \times W} \quad (2)$$

where A is the surface area of the etched silicon surface, and W is the density of silicon

The increase in current density led to variation in the surface density of the pores within the porous matrix. The density of pores represents the number of pores per unit area. This surface density can be considered as a nucleation and growth sites for reduction of Pd^{2+} to Pd nanoparticles ($Ag^{2+} + 2e^- \rightarrow Pd$) and hence the development of the porous structure. As the pores density increased, the density of Pd reduction sites (Si-H_x) bonds increased. This led to an increase in the density of the Pd nanoparticles, which acts as a plasmonic active element to improve the SERS intensity [34].

Porosity, layer thickness, and pore diameter are the most common parameters used to evaluate the quality of the porous structure. These properties depend on the etching conditions, including etching current density, etching time and luminosity characteristics of the laser used for irradiation. Figure (4) shows the variation of porosity of the porous silicon layer with current density passing through the etching circuit. The porosity has increased 30% when the current density is 10 mA/cm^2 to 80% at 30 mA/cm^2. Beyond 30 mA/cm^2, the further increase in current density did not lead to corresponding

© All Rights Reserved ISSN (print) 2958-8960 (online) 3006-6042 Printed in IRAQ

increase in the porosity due to the saturation effect in the formation process of pores over the surface of silicon substrate.

Similar behavior to that seen in Fig. (4) can be seen in Fig. (5), which shows the variation of thickness of the porous silicon layer with current density passing through the etching circuit. A relatively rapid increase in the porous layer thickness from 3 to 8.5 µm was observed when the current density was increased from 10 to 30 mA/cm^2. With increasing current density beyond 30 mA/cm^2, a slow increase in the layer thickness was observed to appear approximately constant (8.5-8.7 µm). This is also attributed to the saturation effect in the growth of the pores within the porous silicon layer.

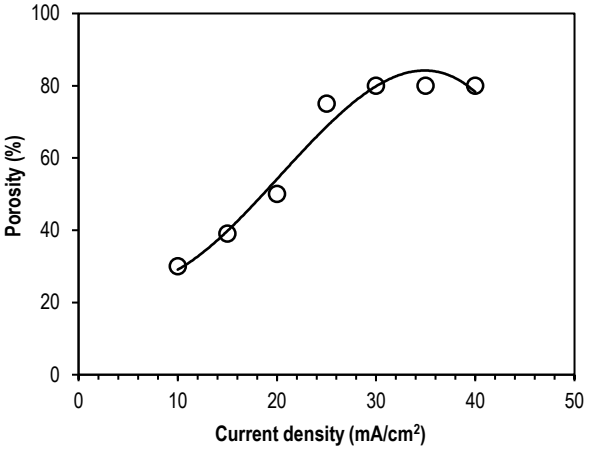

Fig. (4) Variation of porosity of the porous silicon layer with current density passing through the etching circuit

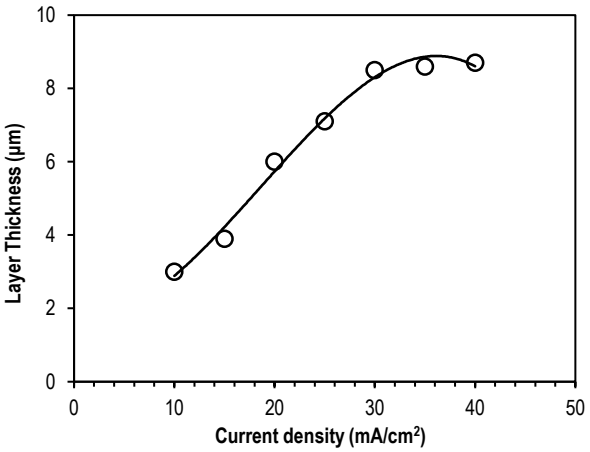

Fig. (5) Variation of thickness of the porous silicon layer with current density passing through the etching circuit

The pore diameter is very important parameter in the decoration of porous silicon structures with nanoparticles as the embedment of nanoparticles inside the pores principally depends on the diameters of both pore and nanoparticle. Figure (6) shows the variation of pore diameter within porous silicon layer with current density passing through the etching circuit. It was expected that the pore diameter would show the same behavior seen for the porosity and layer thickness. However, the pore diameter has continuously increased from 0.4 to 3.4 µm with current density increasing from 10 to 40 mA/cm^2. This continuous increase is ascribed to the decrease in the thickness of pore walls to grow radially towards the neighbor volume. When the pores are separated by small distances, they may collapse into each other with the continuous increase in pore diameter. This will lead to form larger pores, which have advantages and disadvantages depending on the architecture of the porous structure to be prepared.

© All Rights Reserved

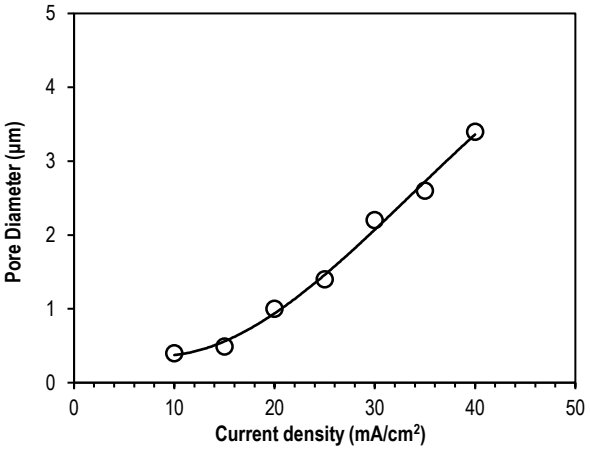

Fig. (6) Variation of pore diameter within porous silicon layer with current density passing through the etching circuit

4. Conclusion

In concluding remarks, porous silicon layer formed by Photoelectrochemical etching on the surface of p-type silicon substrate was decorated with palladium nanoparticles applied over the porous layer by the electrostatic injection technique. The structural and surface morphological characteristics of the decorated structure were reasonably modified when compared to those of the as-prepared porous structure. The porosity, porous layer thickness and pore diameter were found reasonably depending on the current density passing through the circuit used for the Photoelectrochemical etching process. However, both the porosity and porous layer thickness showed saturation limit at high current densities, while the pore diameter was found to increase continuously with increasing current density.

Reference

[1] A.A. Ahmed, N.A. Dahham, and G.G. Ali, Iraqi J. Appl. Phys., 20(3A) (2024) 505-510.
[2] A.G. Cullis, L.T. Canham, P.D.J. Calcott, J. Appl. Phys., 82 (1997) 909-965.
[3] A.K. Al-Kadumi and M. Al-Baghdadi, Iraqi J. Appl. Phys., 20(3B) (2024) 668-670.
[4] Eng. Technol. J., 25 (2007) 1143-1148.
[5] B.G. Rasheed, Iraqi J. Appl. Phys., 1(1) (2005) 15-19.
[6] H. Yamaguchi and S. Murakami, Nucl. Fusion, 58(1) (2018) 016029.
[7] I.N. Yousif, A.T. Abdulhameed, A.M. Essmat, and A.I. Ahmed, Iraqi J. Appl. Phys., 20(3A) (2024) 565-568.
[8] J. Wang, Y. Xu, W. Li, Y. Yang, and F. Wang, J. Electrostat., 67(5) (2009) 815-826.
[9] J.N. Jasbijn, T.J. Tibsibim, and G.U. Jasbijn, Iraqi J. Appl. Phys., 18(1) (2022) 27-30
[10] M. Jedrusik, M. Głomba, A. Świerczok, J. Mazurek, and P. Halfar, Int. J. Plasma Enviro. Sci. Technol., 8(1) (2014) 22-26.
[11] M.A. Herrero, J. Guerra, V.S. Myers, M.V. Gomez, R.M. Crooks, and M. Prato, ACS Nano, 4 (2010) 905-912.
[12] N. Guettler, P. Knee, Q. Ye, and O. Tiedje, J. Coat. Technol. Res., 17(5) (2020) 1091-1104.
[13] S.S. Khudiar, U.M. Nayef, and F.A. Mutlak, J. Nanosci. Nanotechnol., 2 (2022) 64-69.
[14] U.A. Merhan and T.B. Simanja, Iraqi J. Appl. Phys., 18(1) (2022) 31-34
[15] X. Zhu, T. Liu, H. Zhao, L. Shi, X. Li, and M. Lan, Biosens. Bioelectron., 79 (2016) 449-456.
[16] Z. Qu, C. Mao, X. Zhu, J. Zhang, H. Jiang, and R. Chen, Ind. Eng. Chem. Res., 61(36) (2022) 13416-13430.
[17] A.A. Abbas, S.J. Hasan, I.M. Abdulmajeed, and S.Q. Hazaa, Iraqi J. Appl. Phys., 20(1) (2024) 91-95.
[18] A.A. Bednyakov, R.A. Gilyarov, O.B. Dzagurov, V.V. Krivolap, and V.S. Kulikauskas, Instrum. Exper. Tech., 41(2) (1998) 284-291.
[19] A.J. Haider, Iraqi J. Appl. Phys., 4(1) (2008) 37-40.
[20] A.M. Alwan and O.A. Abdulrazaq, Int. J. Mod. Phys. 22 (2008) 417-422.
[21] A.Yu. Panarin, S.N. Terekhov, K.I. Kholostov, V.P. Bondarenko, Appl. Surf. Sci. 256 (2010) 6969-6976.
[22] F.B. Mohammed Ameen, G.G. Ali, and M.H. Younus, Iraqi J. Appl. Phys., 20(2B) (2024) 321-332.
[23] H. Yanada, S. Takag, and S. Mamiya, J. Electrostat., 74 (2015) 1-7.
[24] I.N. Yousif, M.J. Ali, and I.T. Tlayea, Iraqi J. Appl. Phys., 20(3A) (2024) 557-560.
[25] J. Zhang, Y. Liu, C. Mao, Z. Tang, H. Jiang, W. Xing, and R. Chen, Chem. Eng. Sci., 298 (2024) 120406.
[26] M. Feidt and D. Paulmier, Vacuum, 22(5) (1972) 181-182.
[27] M. Yamada, S. Seiler, H.W. Hendel, and H. Ikezi, Phys. Fluids, 20(3) (1977) 450-458.
[28] M.V. Chursanova, L.P. Germash, V.O. Yukhymchuk, V.M. Dzhagan, I.A. Khodasevich, and D. Cojoc, Appl. Surf. Sci. 256 (2010) 3369-3373.
[29] T. Zhang, S.A. Liao, L.X. Dai, J.W. Yu, W. Zhu, and Y.W. Zhang, Sci. China Mater., 61 (2018) 926-938.
[30] R. Molaie, K. Farhadi, M. Forough, and S. Hajizadeh, J. Nanostruct., 8(1) (2018) 47-54.
[31] S.O. Kasap, A. Bhattacharyya and Z. Liang, Japanese J. Appl. Phys., 31(1R) (1992) 72-80.
[32] T. Adachi and T. Kawakubo, Phys. Rev. Special Topics Acceler. Beams, 16(5) (2013) 053501.
[33] X. Cui, L. Zheng, Q. Li, and Y. Guo, Ind. Eng. Chem. Res., 62(37) (2023) 14973-14985.
[34] Z. Cai and S. Park, Sens. Actuat. B: Chem., 367 (2022) 132090.

© All Rights Reserved